

Improved Accuracy and Precision In Simultaneous Myocardial T₁ and T₂ mapping with Multi-Parametric SASHA (mSASHA)

Kelvin Chow¹, Genevieve Hayes², Jacqueline A Flewitt², Patricia Feuchter², Carmen Lydell², Andrew Howarth², Joseph J Pagano³, Richard B Thompson⁴, Peter Kellman⁵, James A White²

¹Cardiovascular MR R&D, Siemens Medical Solutions USA, Inc., Chicago IL, USA

²Stephenson Cardiac Imaging Centre, University of Calgary, Calgary AB, Canada

³Division of Pediatric Cardiology, University of Alberta, Edmonton AB, Canada

⁴Department of Biomedical Engineering, University of Alberta, Edmonton AB, Canada

⁵National Heart, Lung, and Blood Institute, National Institutes of Health, Bethesda MD, USA

This manuscript has been submitted to Magnetic Resonance in Medicine and is under peer review

Running title: Myocardial T₁ and T₂ Mapping with mSASHA

Keywords: T₁ mapping, T₂ mapping, multi-parametric mapping, SASHA, MOLLI, cardiac MR

Data availability statement: The data that support the findings of this study are available from the corresponding author, KC, upon reasonable request.

Corresponding author:

Dr. Kelvin Chow, Cardiovascular MR R&D, Siemens Medical Solutions USA, Inc., Chicago IL, USA

Email: kelvin.chow@siemens-healthineers.com

Abstract

Purpose: To develop and validate a multi-parametric SATuration-recovery single-SHot Acquisition (mSASHA) cardiac T_1 and T_2 mapping technique with high accuracy and precision in a single breath-hold.

Methods: The mSASHA acquisition consists of 9 images in an 11 heartbeat breath-hold -- the first without preparation, 6 images with saturation recovery preparation, and 2 images with both saturation recovery and T_2 -preparation. T_1 and T_2 values were calculated using a 3-parameter model. mSASHA was validated in simulations and phantoms on a Siemens 3T Prisma scanner with comparison to a joint T_1 - T_2 technique with a 4-parameter model. mSASHA values were compared to reference MOLLI, SASHA and T_2 p-bSSFP sequences in 10 healthy volunteers.

Results: mSASHA had high accuracy compared to reference spin-echo measurements, with an average of $-0.7 \pm 0.4\%$ T_1 error and $-1.3 \pm 1.3\%$ T_2 error. mSASHA coefficient of variation (CoV) in phantoms for T_1 was lower than MOLLI ($0.7 \pm 0.1\%$ vs $0.9 \pm 0.2\%$, $p < 0.01$) and similar to reference T_2 p-bSSFP for T_2 ($1.4 \pm 0.6\%$ vs $1.5 \pm 0.5\%$, $p > 0.05$). In simulations, 3-parameter mSASHA fitting had higher precision than 4-parameter joint T_1 - T_2 fitting for both T_1 and T_2 . In-vivo myocardial mSASHA T_1 was similar to conventional SASHA (1523 ± 18 ms vs 1520 ± 18 ms, $p > 0.05$) with similar CoV to both MOLLI and SASHA ($3.3 \pm 0.6\%$ vs $3.1 \pm 0.6\%$ and $3.3 \pm 0.5\%$ respectively, $p > 0.05$ for both). Myocardial mSASHA T_2 values were 37.1 ± 1.1 ms with similar precision to T_2 p-bSSFP ($6.7 \pm 1.7\%$ vs $6.0 \pm 1.6\%$, $p > 0.05$).

Conclusion: mSASHA provides high accuracy cardiac T_1 and T_2 quantification in a single breath-hold, with similar precision to reference MOLLI and linear T_2 p-bSSFP reference techniques.

Background

Cardiac MR is commonly used for the assessment of myocardial disease by measuring abnormalities in tissue relaxation times (1). Increased native longitudinal (T_1) relaxation times have been correlated with myocardial fibrosis (2) and can be combined with post-contrast T_1 imaging to calculate the extracellular volume fraction (ECV) (3-5), a physiologically relevant metric of fibrosis. Increased transverse (T_2) relaxation times have been associated with myocardial edema and inflammation (6). Using conventional, non-parametric, T_1 - and T_2 -weighted imaging techniques, regional myocardial disease is subjectively or semi-quantitatively characterized by relative differences in signal intensity versus reference tissue, the latter assumed to be healthy. However, this poses challenges for the detection of global tissue injury, and inherently limits objective comparisons between individuals and serial evaluations of the same subject. Parametric T_1 and T_2 mapping techniques are intrinsically quantitative, objectively calculating relaxation times in each voxel, eliminating the need for reference tissue comparisons. These address previous challenges of weighted imaging, and optimization of quantitative techniques are focused on increasing imaging efficiency with high accuracy and precision.

T_1 mapping is being increasingly adopted in clinical practice as an quantitative, complementary marker of extracellular matrix expansion, commonly interpreted in parallel with conventional late gadolinium enhancement (LGE) imaging. Two dominant techniques currently exist – the MODified Look-Locker Inversion recovery (MOLLI) sequence (7,8) and the SATuration-recovery single-SHOT Acquisition (SASHA) sequence (9). The MOLLI sequence gained widespread adoption due in part to its high precision and the multitude of studies correlating its T_1 and derived ECV values to various metrics of disease severity in a wide range of cardiomyopathies (4,10-13). However, MOLLI is known to significantly underestimate the true T_1 value, with a bias from physiological parameters such as heart rate (7,14,15), magnetization transfer (16), T_1 (17), T_2 (17) and non-physiological parameters such as inversion pulse efficiency (18), B_0 (19), and B_1 (15) inhomogeneities. By comparison, the SATuration-recovery single-SHOT Acquisition (SASHA) sequence (9) is generally regarded as highly accurate with robustness to confounders such as magnetic field inhomogeneities (B_0 and B_1) (15,20), heart rate (9), T_1 (9), T_2 (9), and magnetization transfer effects (16). However, the original SASHA sequence used a 3-parameter model with lower precision compared to MOLLI due to the reduced dynamic range of saturation recovery approaches compared to inversion recovery techniques (15). Recent work has improved the precision of SASHA using a combination of optimized sampling times (21) and a 2-parameter model with a variable flip angle (VFA) readout (22).

T_2 mapping is commonly performed using a combination of a T_2 preparation (T_2p) pulse and a balanced steady-state free precession (bSSFP) readout with linear k-space ordering (6). This approach is appealing due to its simplicity and high signal-to-noise ratio (SNR), but is known to overestimate T_2 values due to T_1 recovery effects during the imaging readout (6). Centric k-space ordering improves accuracy, but has reduced SNR and also image blurring associated with centric ordering (6).

Several recently developed techniques have combined T_1 and T_2 mapping into a single sequence, including cardiac magnetic resonance fingerprinting (cMRF) (23,24), multitasking (25), joint T_1/T_2 mapping with saturation recovery (26,27), and 3D-QALAS (28). These techniques are attractive because T_1 and T_2 provide complimentary information about tissue microstructure and are often acquired in the same study. Combined multi-parametric techniques also have the unique benefit of being inherently co-registered, avoiding concerns about spatial misalignment when combining data from separate acquisitions. The joint T_1 - T_2 mapping proposed by Akçakaya et al. (26), is a saturation-recovery based sequence similar to SASHA with additional images having T_1 and T_2 preparation. This technique demonstrated good accuracy in phantoms, but had moderate precision due to a 4-parameter fitting model.

In this study, we propose a novel multi-parametric SASHA (mSASHA) sequence that combines T_1 and T_2 mapping in a single saturation-recovery based sequence with improved precision using a 3-parameter model (29). The sequence is validated in simulations and phantoms and then evaluated in healthy subjects alongside the conventional SASHA, MOLLI, and T_2p -bSSFP sequences.

Methods

Theory

The multi-parametric SASHA (mSASHA) acquisition consists of a series of single-shot balanced steady-state free-precession (bSSFP) images, starting with an image without magnetization preparation, followed by a set of saturation-recovery (SR) images, and finally a set of images with both saturation and T_2 -preparation (Fig. 1a). A similar acquisition with combined SR+ T_2p images has been previously described by Akçakaya et al. (26) and Guo et al. (27). The number of SR images and SR+ T_2p images is flexible, with 6 SR images and 2 SR+ T_2p images used in this study for an 11 heartbeat (HB) breath-hold. An additional recovery heartbeat is used between the saturation pulse and T_2p pulses was used to increase the SNR of the SR+ T_2p images.

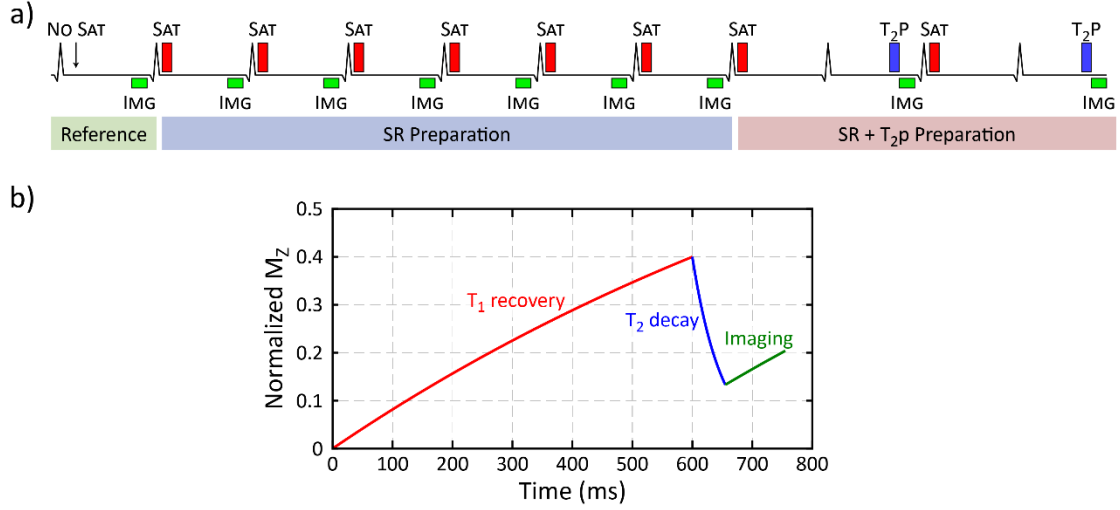


Fig. 1. a) Sequence diagram for multi-parametric SASHA (mSASHA), consisting of a non-prepared reference image, a series of saturation-recovery prepared images, and a series of saturation-recovery and T_2 -prepared images. Imaging is performed using single-shot balanced steady-state free-precession readouts. **b)** Signal model for mSASHA, where the signal intensity for each image is the combination of T_1 recovery, optional T_2 decay, and the effect of the imaging readout.

The longitudinal magnetization for each image can be described as a combination of T_1 weighting from the saturation pulse, optional T_2 weighting from the T_2 -preparation pulse, and an additional effect from the linear bSSFP readout (Fig. 1b). Reference images are a limiting case of full T_1 recovery and no T_2 decay and images with only SR preparation have no T_2 decay component.

In the joint T_1 - T_2 model described by Akçakaya, this can be represented as a 4-parameter equation (Eq. 1) (26):

$$S(T_1, T_2, A, b) = A \left\{ \left(1 - e^{-TS/T_1} \right) e^{-TE/T_2} \right\} + b \quad \text{Eq. 1}$$

Where:

- TS is the saturation recovery time between the end of the saturation pulse and the start of the T_2p pulse for SR+ T_2p images or start of imaging for SR only images,
- TE is the T_2 -preparation duration,
- T_1 is the longitudinal recovery time,
- T_2 is the transverse recovery time, and
- A and b are constants.

In this 4-parameter model, the “b” parameter is a constant offset used to account for the effect of the imaging readout. During a bSSFP readout, the evolution of the longitudinal magnetization can be approximated as exponential recovery with an apparent relaxation rate of (Eq. 2) (30):

$$R_1' = R_1 \cos^2(\theta/2) + R_2 \sin^2(\theta/2) \quad \text{Eq. 2}$$

Where:

- R_1' is the apparent relaxation rate
- R_1 is the true longitudinal relaxation rate, equal to $1/T_1$
- R_2 is the transverse relaxation rate, equal to $1/T_2$
- θ is the bSSFP readout flip angle

Using a partial sinusoidal variable flip angle (VFA) readout, the flip angles prior to the center of k-space are relatively small and R_1' is approximately equal to R_1 . In this case, the signal model can be simplified to 3-parameter one (Eq. 3):

$$S(T_1, T_2, A) = A \left\{ 1 - \left[1 - \left(1 - e^{-TS/T_1} \right) e^{-TE/T_2} \right] e^{-TD/T_1} \right\} \quad \text{Eq. 3}$$

where TD is the known fixed duration between the end of the T_2 preparation pulse and the center of k-space and all other variables are defined as for Eq. 1 and Eq. 2. Data from all images are included during model fitting, where TE=0 is used for images without T_2 preparation.

This 3-parameter (3p) model is hypothesized to improve the precision of calculated T_1/T_2 values compared to the 4-parameter (4p) model due to the simplification of the model. The accuracy and precision of 3p mSASHA is validated with comparison to the 4p joint T_1 - T_2 model in simulations and also to reference standard spin echo in phantom experiments.

Phantom Imaging

Accuracy and precision of the prototype mSASHA sequence was evaluated in a NiCl_2 -doped agarose phantom with physiologic T_1/T_2 combinations representative of myocardium and blood in various physiological and pathological states (T1MES, Resonance Health, Perth, Australia) (31). Imaging was performed on a 3T MAGNETOM Prisma scanner (Siemens Healthcare, Erlangen, Germany). An inversion-recovery spin-echo (IR-SE) acquisition was used for reference T_1 measurements with sequence

parameters: 360×124 mm² field of view, 8 mm slice thickness, 192×66 matrix size, turbo factor 1, echo time (TE) 12 ms, repetition time (TR) 10,000 ms, with 16 inversion times (TI) between 100 and 5,000 ms. Additional spin-echo images were used for reference T₂ measurements with 6 TEs between 12 and 200 ms in separate acquisitions, no inversion, and all other parameters matched.

Conventional cardiac T₁ mapping was also performed in the phantom using the prototype MOLLI and SASHA sequences using a simulated heart rate of 60 bpm and sequence parameters detailed in Table 1. Briefly, MOLLI was acquired with a 5(3)3 sampling scheme and both a typical 35° and a 20° flip angle to reduce sensitivity to B₀/B₁ inhomogeneity. SASHA was acquired with a variable flip angle (VFA) readout with a 70° maximum (22) and a numerically optimized saturation pulse train, providing <1% residual M_z over a wide range of B₀/B₁ (20). Saturation recovery times (TS) for all SR images were set to 600 ms or maximum allowed by heart rate to improve precision (21). Conventional cardiac T₂ mapping was performed using T₂-prepared images with both linear bSSFP and centric gradient recalled echo (GRE) readouts in separate measurements. Linear T₂p-bSSFP protocol parameters are detailed in Table 1 and centric T₂p-GRE images were acquired with a 192×120 matrix size, 83% phase resolution, 1.35/3.20 ms TE/TR, 15° flip angle and all other parameters matched to T₂p-bSSFP.

The proposed mSASHA sequence was acquired with one non-prepared anchor image, 6 SR images with 600 ms TS, and 2 SR+T₂p images with 1600 ms TS and 55 ms T₂p. An optimized T₂-preparation module was used consisting of adiabatic half-passage tan/tanh tip-down and tip-up pulses and 3 adiabatic full-passage tan/tanh refocusing pulses. A 100° maximum VFA readout was used with an additional high-contrast image to improve motion correction (32) and other parameters in Table 1.

As the mSASHA protocol had only two SR+T₂p images with identical T₂p times, the 4-parameter joint T₁-T₂ model was underdetermined and fitting was not possible because only 3 unique TS/T₂p combinations were available. In order to evaluate the precision of 4p joint T₁-T₂ fitting in comparison with mSASHA, a separate 13-heartbeat “variable T₂p” mSASHA dataset was acquired, substituting one of the SR+T₂p images with a 30 ms T₂p duration and adding an SR image with one recovery heartbeat (1600 ms TS).

	Multi-parametric SASHA	SASHA	MOLLI	Linear T ₂ -prepared bSSFP
Field of View	(340-380)×(210-324) mm ²			
Slice Thickness	8 mm			
Matrix Size	256×(118-186)			
Phase Resolution	75%			
Partial Fourier	7/8 th			
Echo Time	1.28-1.31 ms	1.23-1.29 ms	1.09-1.15 ms	1.36-1.42 ms
Repetition Time	2.91-3.04 ms	2.87-3.00 ms	2.64-2.77 ms	3.09-3.23 ms
Flip Angle	100° maximum variable flip angle	70° maximum variable flip angle	20° or 35° constant flip angle (5 linear ramp up pulses)	70° constant flip angle (5 linear ramp up pulse)
Parallel Imaging	R=2, 36 separately acquired reference lines			
Breath-hold duration	11 heartbeats	11 heartbeats	11 heartbeats	9 heartbeats
Sampling Scheme	<ul style="list-style-type: none"> - 1 non-prepared - 6 SR (600 ms TS, or maximum allowed by heart rate) - 2 SR+T₂p (600+RR ms TS, 55 ms T₂p) 	<ul style="list-style-type: none"> - 1 non-prepared - 10 SR (600 ms TS, or maximum allowed by heart rate) 	<ul style="list-style-type: none"> - 5(3)3 scheme - 100 ms minimum TI - 80 ms TI increment 	<ul style="list-style-type: none"> - 0, 30, 55 ms T₂p duration, separated by 3 recovery heartbeats

Table 1. In-vivo protocol parameters for mSASHA, SASHA, MOLLI, and linear T₂-prepared bSSFP sequences for T₁ and T₂ mapping.

Simulations

Monte-Carlo simulations were performed to assess the precision of all fitting models, including the proposed 3-parameter mSASHA model compared to the 4-parameter joint T₁-T₂ model. In order to account for imaging effects on the signal intensity, measured signal intensities from the 13 HB variable T₂p acquisition in the phantoms were used as input for simulations. Simulations were performed for SNR values between 50 and 200 in steps of 25, with 10,000 repeats at each SNR. In each repeat, noise was added to produce a Rician distribution with v being the signal intensities and σ being $1/\text{SNR}$. Data was fit to 3p mSASHA and 4p joint T₁-T₂ models. Data from only the reference and SR images (i.e. excluding SR+T₂p images) were also fit to 2-parameter and 3-parameter SASHA models (T₁ only) for comparison.

In-Vivo Imaging

Ten healthy volunteers with no known history of cardiovascular disease were recruited with written informed consent and imaged on a Siemens 3T MAGNETOM Prisma scanner. mSASHA was acquired in a mid short-axis slice with 6 SR images having a 600 ms TS or maximum allowed by heart rate and both SR+T₂p images having a TS as above with one recovery heartbeat and a 55 ms T₂p. Additional sequence parameters are described in Table 1. MOLLI (both 20° and 35° flip angles), SASHA, and linear T₂p-bSSFP were acquired as reference techniques with parameters as described above. Based on phantom and simulation results, the 13-heartbeat variable T₂p protocol was not acquired in-vivo.

Image Analysis

All images were reconstructed with matched parameters in Gadgetron (33) to facilitate comparison of precision while parametric maps were calculated in MATLAB (R2020a, The MathWorks, Natick, USA). IR-SE T₁ values were calculated using a 3-parameter exponential recovery model and SASHA T₁ values were calculated using a 2-parameter exponential recovery model assuming ideal saturation. MOLLI T₁ values were calculated using a 3-parameter model with Look-Locker correction and an inversion efficiency correction factor of 1.0365 (18). Spin-echo, centric T₂p-GRE, and linear T₂p-bSSFP T₂ values were calculated using a 2-parameter exponential decay model. mSASHA T₁/T₂ values were calculated using the proposed 3-parameter model (Eq. 2). Joint T₁/T₂ values were calculated using 4p joint T₁-T₂ model (Eq. 1) for the variable T₂p data in phantoms, but not the standard mSASHA protocol as the model was underdetermined for these TS/T₂p times. Coefficient of variation (CoV) was calculated for each phantom vial as the standard deviation of T₁ or T₂ over the vial divided by the mean.

In-vivo images from all sequences were motion corrected using the Advanced Normalization Tools (ANTs) software (34), with high-contrast images used to improve motion correction for mSASHA (32). Regions of interest (ROIs) were manually contoured for individual phantom vials, entire left ventricular myocardium, and left ventricular blood pool. T₁ and T₂ values are reported as mean ± standard deviation across the entire ROI. Paired two-sided Student's t-test were used to test for statistical significance with p<0.05.

Results

Phantoms

Measured T_1 and T_2 values from all sequences are reported in Tables 2 and 3 respectively and T_1 and T_2 maps are shown in Fig. 2. The proposed mSASHA with 3-parameter model had excellent T_1 accuracy of $-0.7 \pm 0.4\%$ and T_2 accuracy of $-1.3 \pm 1.3\%$ as compared to spin-echo measurements. Accuracy for the 13-heartbeat variable T_2 p protocol was similar for 3p and 4p models in both T_1 ($-0.7 \pm 0.4\%$ vs $0.2 \pm 0.9\%$, $p > 0.05$) and T_2 fitting ($-2.1 \pm 1.1\%$ vs $3.1 \pm 1.5\%$, $p > 0.05$).

Conventional SASHA had high T_1 accuracy ($-0.9 \pm 0.2\%$) while MOLLI underestimated T_1 values in vials with myocardial-like short T_2 , with increased underestimation at 35° compared to 20° , up to 11.0% error. Centric T_2 p-GRE had good accuracy for most vials except vial 6, where the long T_1 value representative of native blood likely resulted in incomplete magnetization recovery during the recovery interval between images and significant T_2 underestimation. Blurring in the phase encode (vertical) direction is visible in the centric T_2 p-GRE map (Fig. 2), consistent with the centric k-space ordering. Linear T_2 p-bSSFP had significant error for all vials, particularly the ones with post-contrast myocardial-like T_1/T_2 combinations, with up to 78% error.

Parametric map precision in the 13-heartbeat variable T_2 p data was significantly improved using the 3p model compared to the 4p model for both T_1 CoV ($0.6 \pm 0.2\%$ vs. $2.3 \pm 1.3\%$, $p < 0.01$, Table 2) and T_2 CoV ($1.5 \pm 0.7\%$ vs. $3.2 \pm 1.4\%$, $p < 0.01$, Table 3). T_1 CoV with 3p mSASHA ($0.68 \pm 0.14\%$) was similar MOLLI 35° ($0.70 \pm 0.11\%$, $p > 0.05$) and lower than both MOLLI 20° ($0.92 \pm 0.23\%$, $p < 0.01$) and SASHA ($0.76 \pm 0.13\%$, $p < 0.05$). T_2 CoV with 3p mSASHA was not statistically significantly different compared to linear T_2 p-bSSFP ($1.4 \pm 0.6\%$ vs $1.5 \pm 0.5\%$, $p > 0.05$). T_2 precision was not compared with the centric T_2 p-GRE acquisition due to the difference in spatial resolution.

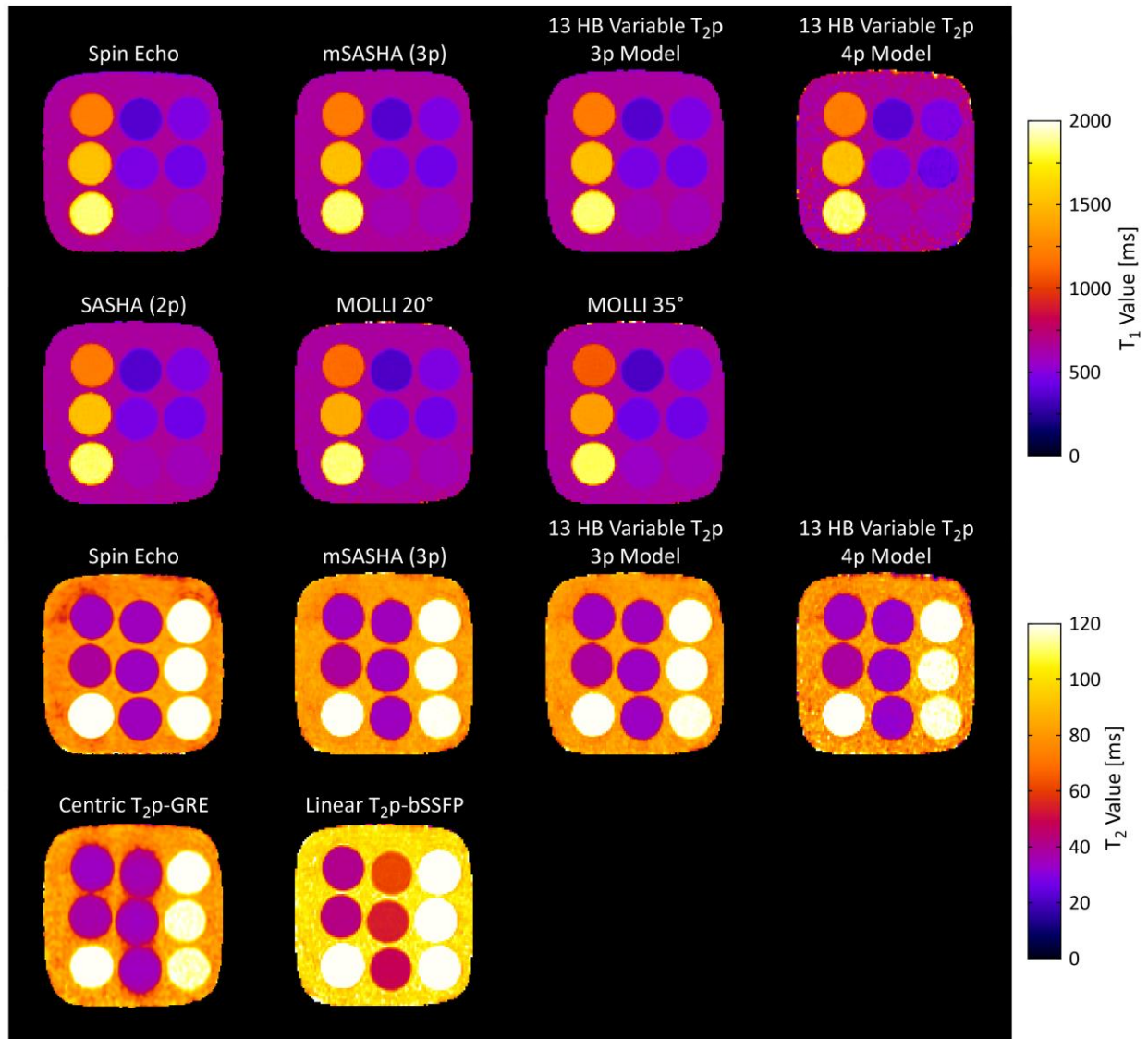


Fig. 2. T_1 and T_2 maps from mSASHA and various reference sequences in a T1MES phantom.

		mSASHA			13 Heartbeat Variable T ₂ p											
	Vial	Spin Echo			3p Model			4p Model			SASHA			MOLLI 20°		
Myocardial-Like	1	1216.7 ± 4.4	1202.8 ± 8.1	1202.9 ± 7.9	1211.5 ± 11.4	1205.7 ± 8.4	1137.0 ± 7.6	1083.3 ± 7.4								
	2	1527.5 ± 9.2	1512.9 ± 13.2	1513.0 ± 12.7	1516.8 ± 19.8	1514.6 ± 13.4	1429.9 ± 10.7	1360.9 ± 9.8								
	3	606.4 ± 2.9	601.3 ± 4.1	600.9 ± 4.2	614.2 ± 13.9	601.6 ± 4.9	571.4 ± 7.3	553.9 ± 5.2								
	4	470.9 ± 2.2	465.8 ± 3.5	465.6 ± 3.1	473.1 ± 7.7	465.9 ± 3.7	442.2 ± 5.3	434.1 ± 2.9								
	5	365.1 ± 2.0	361.2 ± 2.4	361.1 ± 2.1	367.6 ± 4.5	360.7 ± 2.6	344.1 ± 3.0	340.0 ± 2.3								
Blood-Like	6	1856.7 ± 10.9	1850.5 ± 15.6	1850.7 ± 14.9	1852.3 ± 30.2	1842.5 ± 18.5	1855.4 ± 15.9	1829.5 ± 10.7								
	7	590.7 ± 1.4	590.5 ± 3.9	590.6 ± 3.5	592.7 ± 21.0	587.2 ± 4.2	594.1 ± 6.4	590.9 ± 4.5								
	8	441.8 ± 1.4	439.7 ± 2.6	440.3 ± 2.2	436.3 ± 21.5	437.9 ± 3.2	441.3 ± 4.2	441.1 ± 3.2								
	9	483.1 ± 1.1	479.7 ± 1.9	480.3 ± 1.7	475.4 ± 13.5	478.6 ± 2.5	482.8 ± 3.1	482.2 ± 2.6								

Table 2. T₁ measurements with various sequences in NiCl₂ doped agarose phantom. Values are reported as mean ± standard deviation across each vial. Coefficients of variation (CoV) were calculated as standard deviations divided by means.

		mSASHA			13 Heartbeat Variable T ₂ p						Centric			Linear		
	Vial	Spin Echo			3p Model			4p Model			T ₂ p-GRE			T ₂ p-bSSFP		
Myocardial-Like	1	34.6 ± 0.2	34.4 ± 0.3	34.1 ± 0.3	33.9 ± 0.5	34.0 ± 0.3	40.8 ± 0.3									
	2	39.3 ± 0.2	38.9 ± 0.5	38.6 ± 0.4	38.5 ± 0.5	37.1 ± 0.4	42.2 ± 0.4									
	3	34.6 ± 0.4	34.2 ± 0.5	33.9 ± 0.4	32.8 ± 1.2	34.3 ± 0.4	48.6 ± 0.6									
	4	34.1 ± 0.2	34.2 ± 0.4	33.8 ± 0.3	32.8 ± 1.0	34.5 ± 0.5	53.8 ± 0.6									
	5	34.6 ± 0.3	34.9 ± 0.3	34.5 ± 0.3	33.0 ± 1.0	36.1 ± 0.4	61.5 ± 0.6									
Blood-Like	6	203.7 ± 1.4	198.4 ± 5.1	198.4 ± 6.1	198.5 ± 6.5	132.6 ± 3.1	172.4 ± 3.5									
	7	125.0 ± 0.9	120.9 ± 1.7	119.8 ± 1.8	119.6 ± 3.9	115.6 ± 2.4	142.4 ± 2.8									
	8	127.1 ± 0.9	124.3 ± 1.4	123.6 ± 1.4	125.6 ± 7.7	118.2 ± 1.8	155.0 ± 2.6									
	9	129.8 ± 2.9	127.2 ± 2.7	126.3 ± 2.8	127.8 ± 5.1	123.4 ± 1.9	155.8 ± 3.5									

Table 3. T₂ measurements with various sequences in NiCl₂ doped agarose phantom. Values are reported as mean ± standard deviation across each vial. Coefficients of variation (CoV) were calculated as standard deviations divided by means.

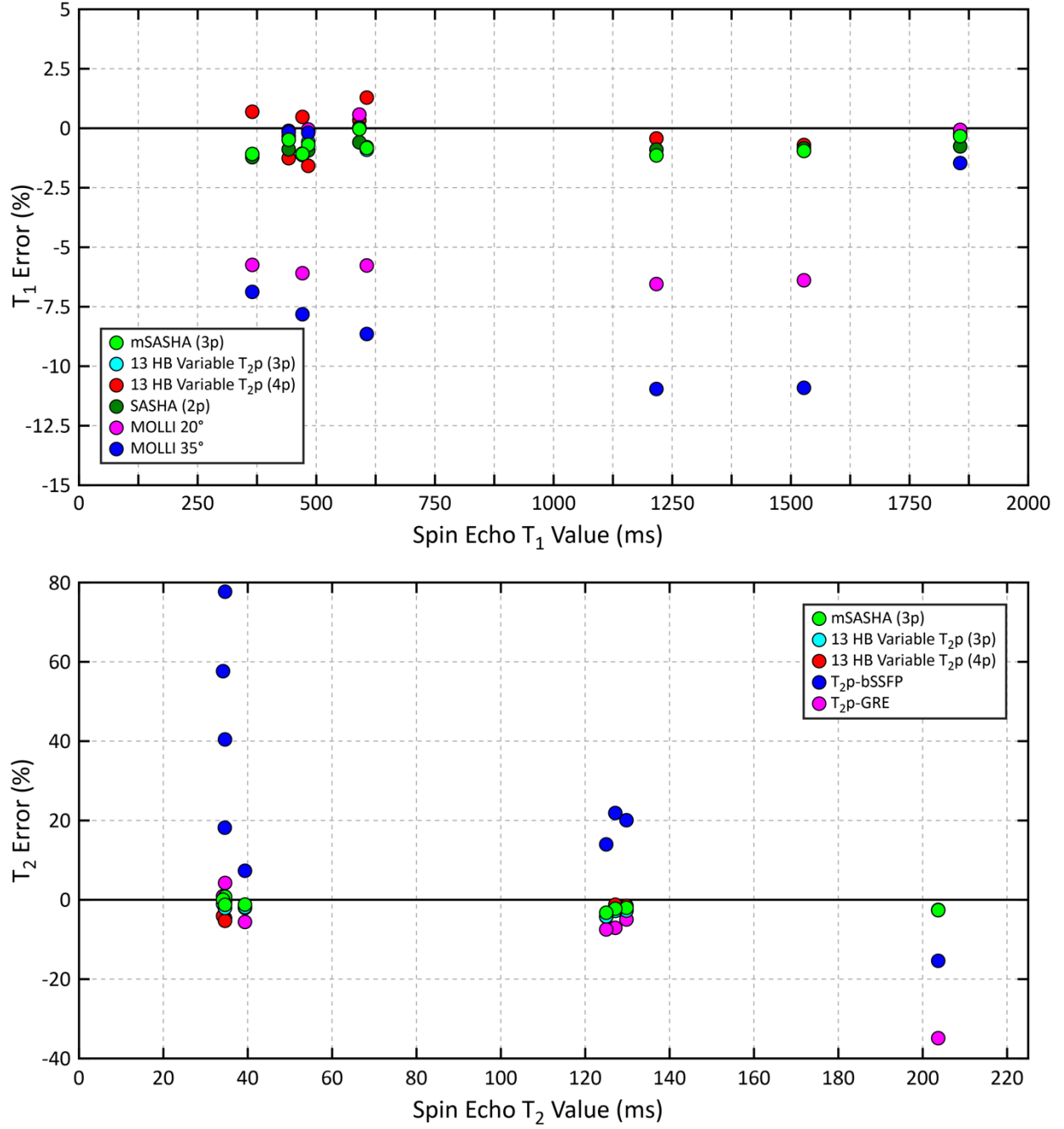


Fig. 3. Accuracy of mSASHA T_1/T_2 and various reference sequences compared to gold standard spin-echo measurements. Accuracy for 13 HB variable T_2p with 3p fitting is very similar to mSASHA (3p) and plotted data points are largely obscured.

Simulations

Monte-Carlo simulations of precision (Fig. 4) were consistent with phantom data. In the native myocardium (vial 1) and blood (vial 6) simulations, the T_1 IQR of 4p joint T_1 - T_2 was similar to 3p SASHA as previously described (26) and T_1 IQR of 3p mSASHA was similar to 2p SASHA. In both cases, T_1 precision was not adversely affected by the use of combined T_1 / T_2 models compared to T_1 -only fitting models. The T_1 IQR at an SNR of 100 for 4p joint T_1 - T_2 was 2.6 \times and 2.4 \times worse than 3p mSASHA for native myocardium and blood, respectively. Both 4p joint T_1 - T_2 and 3p SASHA had significantly higher IQR compared to 3p mSASHA when T_1 was short or T_2 was long due to ill conditioning of these models with the TS/T_2 p times used. Overall, 3p mSASHA had more robust precision over a range of T_1 / T_2 values.

T_2 precision with 3p mSASHA was superior to 4p joint T_1 - T_2 in all cases (Fig. 4), with T_2 IQR with 4p joint T_1 - T_2 being 1.7 \times larger for native myocardium and 1.1 \times larger for native blood. However, T_2 IQR with 4p joint T_1 - T_2 was substantially worse than 3p mSASHA in simulations with short T_1 representing post-contrast imaging.

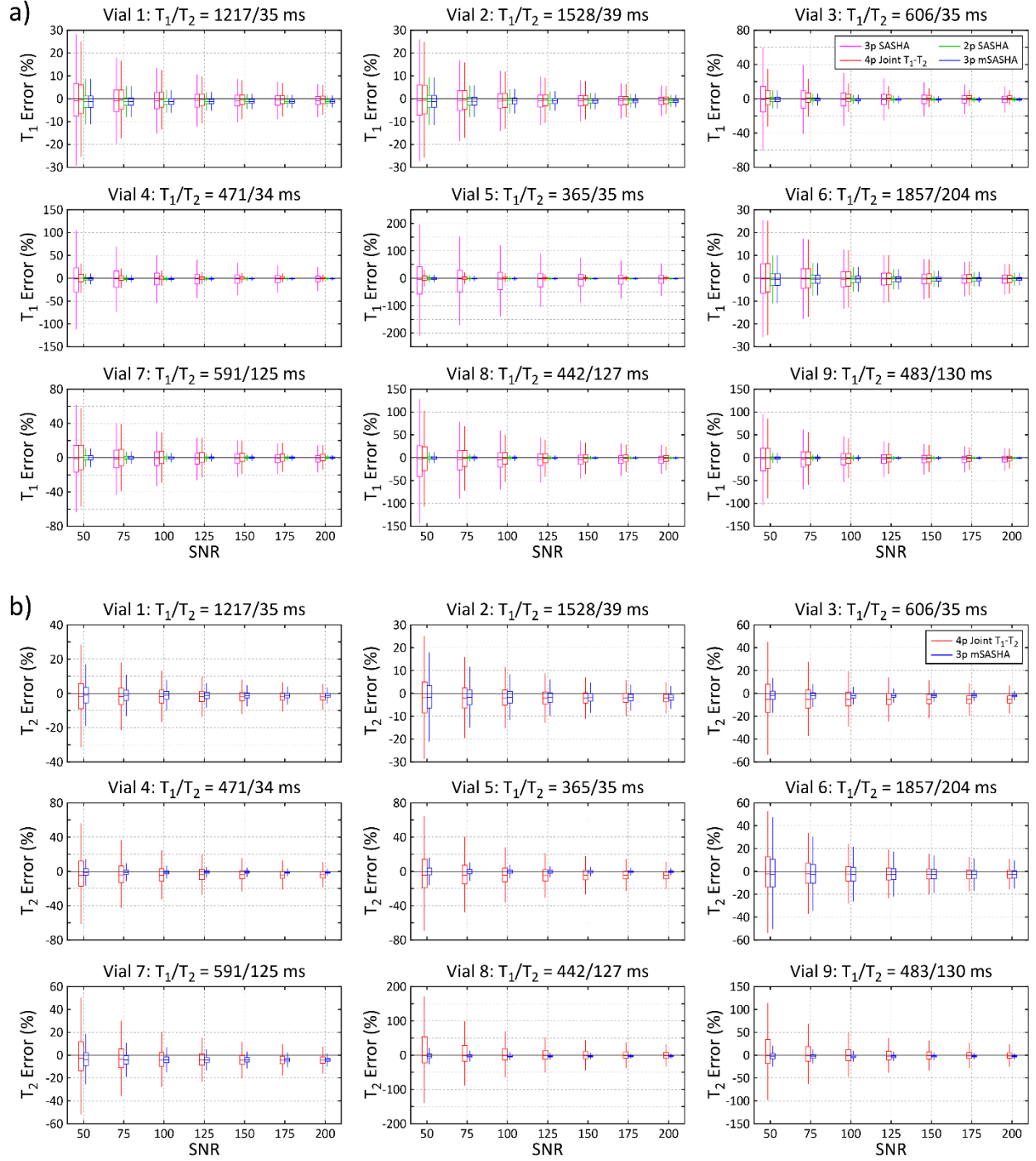


Fig. 4. Monte Carlo simulation results of **a)** T_1 and **b)** T_2 precision with various signal models. Boxes indicate the first and third quartiles and whiskers indicate $1.5 \times \text{IQR}$.

In-Vivo

Volunteers were an average of 44.2 ± 13.1 years old (7 female) with a heart rate of 69 ± 12 bpm during imaging. MOLLI 20° data from one subject was discarded due to operator error (insufficient recovery period prior to start of acquisition). T_1 and T_2 values from all sequences are detailed in Table 4 and T_1 and T_2 maps from all sequences in a healthy volunteer are shown in Fig. 5. mSASHA T_1 values were not statistically significantly different from SASHA T_1 values for both the myocardium (1523 ± 18 ms vs 1520 ± 18 , $p > 0.05$) and left ventricular blood pool (2054 ± 61 ms vs 2060 ± 65 ms, $p > 0.05$). MOLLI T_1 values were underestimated in the myocardium compared to SASHA, with greater underestimation at 35° than 20° (1218 ± 23 ms vs 1275 ± 24 ms, $p < 0.001$). T_2 values with linear T_2 p-bSSFP were higher than mSASHA in the myocardium (41.3 ± 1.7 ms vs 36.7 ± 1.1 ms, $p < 0.001$) but lower in the blood (127.9 ± 9.8 ms vs 160.8 ± 14.8 ms, $p < 0.001$), consistent with over/underestimation observed in phantoms for similar T_1/T_2 combinations.

The CoV for mSASHA T_1 values was not statistically significantly different than SASHA in both the myocardium and blood pool ($p > 0.05$, Table 4). Myocardial mSASHA T_1 CoV ($3.3 \pm 0.6\%$) was not statistically significantly different than either MOLLI 20° ($3.1 \pm 0.6\%$) or MOLLI 35° ($3.3 \pm 0.8\%$) ($p > 0.05$ for both). However, mSASHA T_1 CoV in the blood ($3.0 \pm 0.7\%$) was larger than both MOLLI 20° ($2.0 \pm 0.4\%$) and MOLLI 35° ($1.6 \pm 0.3\%$) ($p < 0.001$ for both). T_2 CoV was not statistically significantly different between mSASHA and linear T_2 p-bSSFP in both the myocardium ($6.7 \pm 1.0\%$ vs $6.0 \pm 1.6\%$, $p > 0.05$) and the blood ($9.8 \pm 4.0\%$ vs $9.1 \pm 3.1\%$, $p > 0.05$).

	T ₁ Values								T ₂ Values			
	mSASHA		SASHA		MOLLI 20°		MOLLI 35°		mSASHA		Linear T ₂ p-bSSFP	
Myocardial value (ms)	1523.1 ±	17.8	1519.5 ±	18.0	1275.0 ±	23.9	1217.7 ±	22.9	36.7 ±	1.1	41.3 ±	1.7
Blood value (ms)	2054.1 ±	60.9	2060.1 ±	65.4	1872.7 ±	71.4	1855.7 ±	64.1	160.8 ±	14.8	127.9 ±	9.8
Myocardial SD (ms)	50.7 ±	9.4	49.6 ±	7.2	40.0 ±	7.4	40.7 ±	9.5	2.5 ±	0.6	2.5 ±	0.7
Blood SD (ms)	62.7 ±	14.9	64.5 ±	16.0	37.5 ±	7.6	29.4 ±	5.6	16.0 ±	7.4	11.7 ±	4.3
Myocardial CoV (%)	3.3 ±	0.6	3.3 ±	0.5	3.1 ±	0.6	3.3 ±	0.8	6.7 ±	1.7	6.0 ±	1.6
Blood CoV (%)	3.0 ±	0.7	3.1 ±	0.8	2.0 ±	0.4	1.6 ±	0.3	9.8 ±	4.0	9.1 ±	3.1

Table 4. T₁ and T₂ measurements in 10 healthy volunteers with mSASHA, SASHA, MOLLI, and linear T₂p-bSSFP.

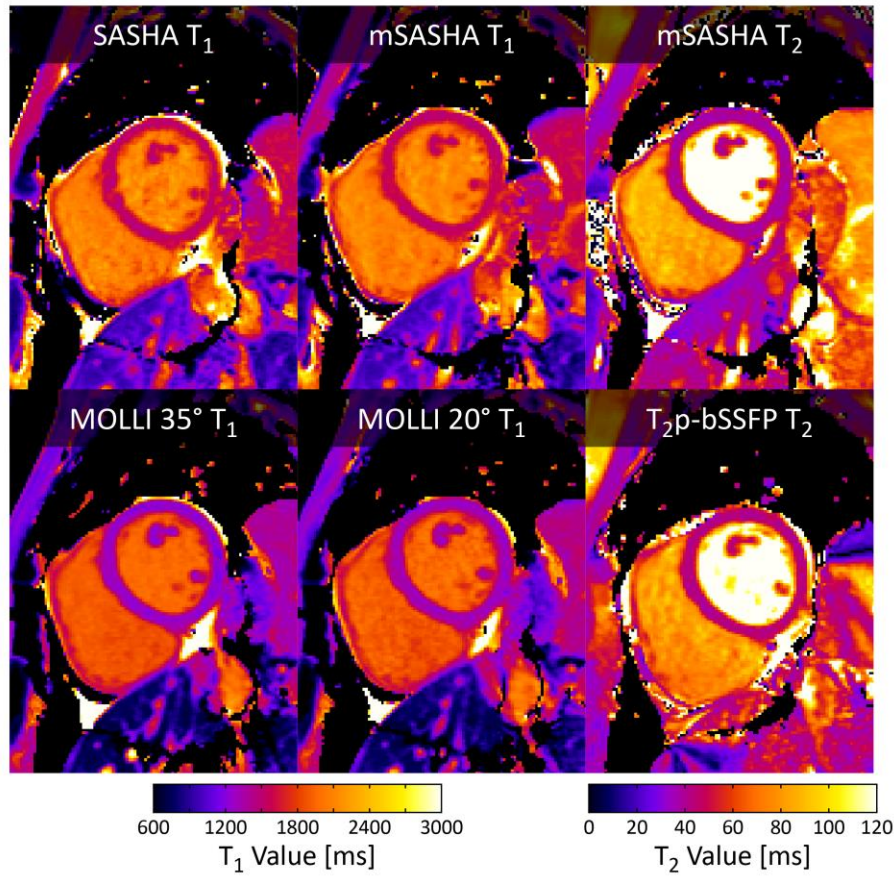


Fig. 5. T₁ and T₂ maps from mSASHA, SASHA, MOLLI, and linear T₂p-bSSFP sequences in a healthy subject at 3T.

Discussion

We demonstrated mSASHA to be a robust and clinically translatable technique that maintains the superior accuracy and precision of the SASHA T_1 mapping sequence while providing simultaneous T_2 quantification in a single breath-hold. Use of a variable flip angle readout enabled formulation of a 3-parameter model for simultaneous T_1 and T_2 mapping with multi-parametric SASHA, significantly improving precision compared to the 4-parameter joint T_1 - T_2 model (26,27). Overall, mSASHA resulted in the lowest T_1 and T_2 error (<1.5%) in phantoms and maintained in-vivo precision similar to that provided by the most commonly used MOLLI T_1 and linear T_2 p-bSSFP clinical sequences.

Simultaneous and accurate quantification of T_1 and T_2 enables improved characterization of microstructural changes encountered with myocardial disease. The widely used MOLLI T_1 mapping sequence is recognized to be confounded by alterations in T_2 (15,17), while linear T_2 p-bSSFP values are conversely confounded by T_1 (6). In contrast, mSASHA provided accurate quantification of both T_1 and T_2 across a wide range of physiologically relevant T_1 / T_2 combinations, enabling each parameter to be reliably measured even if the other is altered. The intrinsic co-registration of mSASHA T_1 and T_2 maps may be particularly useful in the assessment of the area-at-risk, as fibrosis and edema-mediated microstructural changes may provide unique influences on these respective parameters. Simultaneous and accurate measurements may also permit improved understanding of the relationship between T_1 and T_2 changes across a variety of myocardial disease states, including of inflammatory myocarditis, iron overload, and genetically-mediated cardiomyopathies.

Comparisons with Other Parametric Mapping Sequences

Several alternative sequences exist for simultaneous cardiac T_1 and T_2 quantification. The joint T_1 and T_2 mapping sequence proposed by Akçakaya et al. (26) has several similarities to mSASHA as they both use a similar single-shot bSSFP acquisition with variable saturation and T_2 -preparation modules. However, the reduction in the number of fit parameters with 3p mSASHA compared to 4p joint T_1 - T_2 significantly improved precision in both Monte Carlo simulations and phantom data. T_1 precision of 4p joint T_1 - T_2 was comparable to T_1 -only 3-parameter SASHA fitting in simulations, consistent with reports by Akçakaya et al. and Guo et al. (26,27). The improved precision of 2p SASHA versus 3p SASHA is also consistent with previous literature (15,22). Precision for 4p joint T_1 - T_2 and 3p SASHA was poor for short T_1 and long T_2 combinations due to poor sampling of the recovery curve. Precision could potentially be

improved for these models through optimization of the T_2/T_2^* sampling times (21,35) for different expected T_1/T_2 values, such as different sampling schemes for native and post-contrast. In contrast, precision of 3p mSASHA was stable across simulations in all phantom vials.

With respect to in-vivo T_1 values obtained using joint versus separate acquisition sequences, Akçakaya et al., previously found similar mean values between joint T_1 and SASHA T_1 in-vivo at 1.5T (26). However, a recent multi-slice extension of the joint T_1 - T_2 approach by Guo et al. at 3T showed significant underestimation of T_1 values compared to SASHA (191 ms in volunteers, 111 ms in patients), with unknown causes (27). In our study, we observed no underestimation of in-vivo mSASHA T_1 values vs SASHA (1523 ± 18 ms vs 1520 ± 18 ms, $p > 0.05$). These values were also similar to literature values for SASHA at 3T, with Weingärtner et al. measuring 1523 ± 41 ms in 20 volunteers (36), Guo et al. reporting 1521 ± 17 ms in the basal slice of 13 healthy volunteers (27), and Heidenreich et al. describing 1460 ± 67 ms in remote myocardium of 19 patients (37). Agreement between mSASHA and SASHA in both simulations and previously published in-vivo SASHA values suggests that reference normal values from SASHA could potentially be used for mSASHA as well. However, further comparison in a larger population is required to confirm their equivalence. mSASHA myocardial T_2 values in this study (36.7 ± 1.1 ms) were similar to previously reported values at 3T with gradient echo based techniques by van Heeswijk et al. (38.5 ± 4.5 ms) (38) and Yang et al. (37.7 ± 2.0 ms) (39).

Multi-parametric cardiac mapping techniques with novel and advanced reconstruction approaches have also been recently proposed to combine T_1 and T_2 mapping with cine imaging. CMR multitasking T_1 - T_2 mapping combines a hybrid T_2 IR prepared free-breathing continuous radial acquisition with a low-rank tensor model to calculate cardiac phase resolved T_1 and T_2 maps (25). CMR fingerprinting additionally uses inversion and T_2 -preparation pulses combined with a variable flip angle pattern to induce magnetization evolutions characteristic of T_1/T_2 combinations that can be matched to a simulated dictionary (23,24). These techniques are appealing due to their free-breathing acquisition and the additional cardiac phase dimension, however are dependent on the validity of assumptions made in the modeled reconstruction. Reported in-vivo T_1 values from multitasking and CMR fingerprinting are similar to MOLLI (23,25), suggesting these techniques may also be susceptible to confounders.

In contrast, mSASHA uses a straightforward model with single-shot images having well-defined T_1 and T_2 weighting. Saturation pulses preceding each weighted image “reset” the magnetization to zero and remove interdependence between images as a potential confounding factor. This simplistic model has fewer assumptions and may therefore be more robust to unknown confounders. Techniques such as

multitasking and fingerprinting utilize modeling of the magnetization history to calculate additional parameters, but can be subject to error when additional influences on signal evolution are not included in the model. For example, MOLLI is significantly affected by magnetization transfer (MT) because the cumulative effects of MT through each image readout is carried over to subsequent images (16). For continuous 2D implementations of multitasking and fingerprinting, through-plane motion may also present a challenging confounder to mitigate.

The Need For Accurate Parametric Mapping

While absolute accuracy itself is a laudable goal for parametric mapping sequences, measurement precision is often prioritized in clinical translational research. The eventual desired application of such techniques is identification of disease through abnormalities in parametric values relative to a normal reference range. Methods with higher precision narrow this range, enabling detection of more subtle deviations from a state of health, while accuracy shifts actual values for this range.

However, an understanding of the underlying mechanisms behind inaccurate measurements is important for the robustness of a method as it matures beyond small single-center studies. MOLLI's underestimation is due to a complex interaction of both physiological factors such as heart rate, T_1 , T_2 , and magnetization transfer, protocol parameters such as flip angle and number of phase encode lines, as well as B_0 and B_1 field inhomogeneities (15). Linear T_2 p-bSSFP errors are primarily due to T_1 recovery during imaging, which is determined by the number of phase encode lines, and heart rate for long T_1 species. In general, confounders leading to inaccuracies are not constant and can be influenced by the sequence implementation, the operator's choice of protocol parameters, and other physiological factors. These factors are often difficult to control, particularly outside of single-center focused research studies, and reducing confidence that T_1/T_2 abnormalities reflect actual physiological changes. For sequences with known biases but unknown causes, it is even more challenging to confidently attribute measured T_1/T_2 changes to microstructural changes instead of underlying confounders.

The consensus statement from the parametric mapping working group recommends that each site establish normal values for each sequence and protocol to reduce the impact of such confounders (40). While necessary given the confounders present in many existing sequences, protocol parameters often must be changed in response to the patient's habitus or heart rate and does not fully address

physiological confounders. Furthermore, this presents a significant burden for clinicians and confusion about sequence specific normative values limits the widespread adoption of parametric mapping overall.

A significant practical benefit of accurate sequences is that the measured normal values in healthy subjects are, by definition, the intrinsic T_1 and T_2 values instead of a combination of the true value and that sequence's confounding factors. Ongoing development and validation of accurate mapping sequences that are robust enough to not require site-specific normative values would significantly reduce the burden for more widespread translation of parametric mapping into clinical practice. Abnormalities in T_1 or T_2 values could also be more confidently ascribed to physiological changes instead of confounding factors.

Limitations

mSASHA extends upon the well validated and robust SASHA sequence and data in this study reaffirms its accuracy in phantoms with similar in-vivo T_1 values. Although there are no known significant confounders to the SASHA sequence, further study is required to similarly validate the mSASHA sequence. The variable flip angle readout enables the use of the 3-parameter model, but also results in an asymmetric modulation transfer function (MTF) across k-space. However, image sharpness in phantoms and in-vivo data did not appear to be significantly affected. Similar to many conventional techniques, mSASHA uses a single-shot readout that can be affected by cardiac motion at high heart rates and optimization of the readout and sampling strategies for higher heart rates is needed.

The in-vivo study was limited to a small cohort of healthy subjects and additional studies in a more diverse population of patients is required to assess its robustness in a more challenging clinical environment. The study was also limited to non-contrast imaging and further comparisons in subjects post-gadolinium contrast should be performed to determine relative precision and overall performance of mSASHA in-vivo with shorter T_1/T_2 values. mSASHA was compared only to a limited subset of widely used T_1 and T_2 mapping techniques and comparisons to newer techniques such as multitasking and cMRF would be valuable in the future.

Conclusions

Multi-parametric mSASHA provides accurate and precise simultaneous T_1 and T_2 quantification in a single breath-hold, delivering voxel-registered myocardial tissue characterization with reduced scan times. Further study with mSASHA is required to establish normative values at both 1.5 and 3T and demonstrate the potential of co-registered T_1 and T_2 voxel profiles to characterize and prognosticate cardiomyopathy states.

References

1. Leiner T, Bogaert J, Friedrich MG, Mohiaddin R, Muthurangu V, Myerson S, Powell AJ, Raman SV, Pennell DJ. SCMR Position Paper (2020) on clinical indications for cardiovascular magnetic resonance. *J Cardiovasc Magn Reson* 2020;22:1–37. doi: 10.1186/s12968-020-00682-4.
2. Bull S, White SK, Piechnik SK, et al. Human non-contrast T1 values and correlation with histology in diffuse fibrosis. *Heart* 2013;99:932–937. doi: 10.1136/heartjnl-2012-303052.
3. Flacke SJ, Fischer SE, Lorenz CH. Measurement of the gadopentetate dimeglumine partition coefficient in human myocardium in vivo: normal distribution and elevation in acute and chronic infarction. *Radiology* 2001;218:703–710.
4. Ugander M, Oki AJ, Hsu L-Y, Kellman P, Greiser A, Aletras AH, Sibley CT, Chen MY, Bandettini WP, Arai AE. Extracellular volume imaging by magnetic resonance imaging provides insights into overt and sub-clinical myocardial pathology. *European heart journal* 2012;33:1268–1278. doi: 10.1093/eurheartj/ehr481.
5. Sado DM, Flett AS, Banypersad SM, et al. Cardiovascular magnetic resonance measurement of myocardial extracellular volume in health and disease. *Heart* 2012;98:1436–1441. doi: 10.1136/heartjnl-2012-302346.
6. Giri S, Chung Y-C, Merchant A, Mihai G, Rajagopalan S, Raman SV, Simonetti OP. T2 quantification for improved detection of myocardial edema. *J Cardiovasc Magn Reson* 2009;11:56. doi: 10.1186/1532-429X-11-56.
7. Messroghli DR, Radjenovic A, Kozerke S, Higgins DM, Sivananthan MU, Ridgway JP. Modified Look-Locker inversion recovery (MOLLI) for high-resolution T1 mapping of the heart. *Magn Reson Med* 2004;52:141–146. doi: 10.1002/mrm.20110.
8. Messroghli DR, Greiser A, Fröhlich M, Dietz R, Schulz-Menger J. Optimization and validation of a fully-integrated pulse sequence for modified look-locker inversion-recovery (MOLLI) T1 mapping of the heart. *J Magn Reson Imaging* 2007;26:1081–1086. doi: 10.1002/jmri.21119.

9. Chow K, Flewitt JA, Green JD, Pagano JJ, Friedrich MG, Thompson RB. Saturation recovery single-shot acquisition (SASHA) for myocardial T1 mapping. *Magn Reson Med* 2014;71:2082–2095. doi: 10.1002/mrm.24878.
10. Mewton N, Liu CY, Croisille P, Bluemke DA, Lima JAC. Assessment of myocardial fibrosis with cardiovascular magnetic resonance. *J Am Coll Cardiol* 2011;57:891–903. doi: 10.1016/j.jacc.2010.11.013.
11. Bulluck H, Maestrini V, Rosmini S, Abdel-Gadir A, Treibel TA, Castelletti S, Bucciarelli-Ducci C, Manisty C, Moon JC. Myocardial T1 mapping. *Circ. J.* 2015;79:487–494. doi: 10.1253/circj.CJ-15-0054.
12. de Meester de Ravenstein C, Bouzin C, Lazam S, et al. Histological Validation of measurement of diffuse interstitial myocardial fibrosis by myocardial extravascular volume fraction from Modified Look-Locker imaging (MOLLI) T1 mapping at 3T. *J Cardiovasc Magn Reson* 2015;17:48. doi: 10.1186/s12968-015-0150-0.
13. Reiter U, Reiter C, Kräuter C, Fuchsjäger M, Reiter G. Cardiac magnetic resonance T1 mapping. Part 2: Diagnostic potential and applications. *Eur J Radiol* 2018;109:235–247. doi: 10.1016/j.ejrad.2018.10.013.
14. Lee JJ, Liu S, Nacif MS, Ugander M, Han J, Kawel N, Sibley CT, Kellman P, Arai AE, Bluemke DA. Myocardial T1 and extracellular volume fraction mapping at 3 tesla. *J Cardiovasc Magn Reson* 2011;13:75. doi: 10.1186/1532-429X-13-75.
15. Kellman P, Hansen MS. T1-mapping in the heart: accuracy and precision. *J Cardiovasc Magn Reson* 2014;16:2. doi: 10.1186/1532-429X-16-2.
16. Robson MD, Piechnik SK, Tunnicliffe EM, Neubauer S. T1 measurements in the human myocardium: The effects of magnetization transfer on the SASHA and MOLLI sequences. *Magn Reson Med* 2013;70:–670. doi: 10.1002/mrm.24867.
17. Chow K, Flewitt JA, Pagano JJ, Green JD, Friedrich MG, Thompson RB. MOLLI T1 Values Have Systematic T2 and Inversion Efficiency Dependent Errors. *Proc Intl Soc Magn Reson Med* 2012. p. 395.
18. Kellman P, Herzka DA, Hansen MS. Adiabatic inversion pulses for myocardial T1 mapping. *Magn Reson Med* 2014;71:1428–1434. doi: 10.1002/mrm.24793.

19. Kellman P, Herzka DA, Arai AE, Hansen MS. Influence of Off-resonance in myocardial T1-mapping using SSFP based MOLLI method. *J Cardiovasc Magn Reson* 2013;15:63. doi: 10.1186/1532-429X-15-63.
20. Chow K, Kellman P, Spottiswoode BS, Nielles-Vallespin S, Arai AE, Salerno M, Thompson RB. Saturation pulse design for quantitative myocardial T 1 mapping. *J Cardiovasc Magn Reson* 2015;17:84. doi: 10.1186/s12968-015-0187-0.
21. Kellman P, Xue H, Chow K, Spottiswoode BS, Arai AE, Thompson RB. Optimized saturation recovery protocols for T1-mapping in the heart: influence of sampling strategies on precision. *J Cardiovasc Magn Reson* 2014;16:55. doi: 10.1186/s12968-014-0055-3.
22. Chow K, Spottiswoode B, Pagano JJ, Thompson R. Improved precision in SASHA T1 mapping with a variable flip angle readout. *J Cardiovasc Magn Reson* 2014;16:M9.
23. Hamilton JI, Jiang Y, Chen Y, Ma D, Lo WC, Griswold MA, Seiberlich N. MR fingerprinting for rapid quantification of myocardial T1, T2, and proton spin density. *Magn Reson Med* 2017;77:1446–1458. doi: 10.1002/mrm.26216.
24. Hamilton JI, Jiang Y, Eck B, Griswold MA, Seiberlich N. Cardiac cine magnetic resonance fingerprinting for combined ejection fraction, T1 and T2 quantification. *NMR Biomed* 2020;33. doi: 10.1002/nbm.4323.
25. Christodoulou AG, Shaw JL, Nguyen C, Yang Q, Xie Y, Wang N, Li D. Magnetic resonance multitasking for motion-resolved quantitative cardiovascular imaging. *Nat Biomed Eng* 2018;2:215–226. doi: 10.1038/s41551-018-0217-y.
26. Akçakaya M, Weingärtner S, Basha TA, Roujol S, Bellm S, Nezafat R. Joint myocardial T1 and T2 mapping using a combination of saturation recovery and T2-preparation. *Magn Reson Med* 2016;76:888–896. doi: 10.1002/mrm.25975.
27. Guo R, Cai X, Kucukseymen S, Rodriguez J, Paskavitz A, Pierce P, Goddu B, Thompson RB, Nezafat R. Free-breathing simultaneous myocardial T 1and T 2mapping with whole left ventricle coverage. *Magn Reson Med* 2020;mrm.28506.
28. Kvernby S, Warntjes MJ, Haraldsson H, Carlhäll C-J, Engvall J, Ebberts T. Simultaneous three-dimensional myocardial T1 and T2 mapping in one breath hold with 3D-QALAS. *J Cardiovasc Magn Reson* 2014;16:102. doi: 10.1186/s12968-014-0102-0.

29. Chow K, Hayes G, Flewitt JA, Feuchter P, Lydell CP, Howarth A, Pagano JJ, Thompson RB, Kellman P, White JA. Accurate and precise myocardial T1 and T2 mapping in a single breath-hold with multi-parametric SASHA. *Proc Intl Soc Mag Reson Med*. 2021:4046.
30. Scheffler K. On the transient phase of balanced SSFP sequences. *Magn Reson Med* 2003;49:781–783. doi: 10.1002/mrm.10421.
31. Captur G, Gatehouse PD, Heslinga FG, et al. A T1 and ECV phantom for global T1 mapping quality assurance: The T1 mapping and ECV standardisation in CMR (T1MES) program. *J Cardiovasc Magn Reson* 2016;18:W18–571.
32. Chow K, Yang Y, Shaw P, Kramer CM, Salerno M. Robust free-breathing SASHA T1 mapping with high-contrast image registration. *J Cardiovasc Magn Reson* 2016;18:47. doi: 10.1186/s12968-016-0267-9.
33. Hansen MS, Sørensen TS. Gadgetron: An open source framework for medical image reconstruction. *Magn Reson Med* 2013;69:1768–1776. doi: 10.1002/mrm.24389.
34. Avants BB, Tustison NJ, Song G, Cook PA, Klein A, Gee JC. A reproducible evaluation of ANTs similarity metric performance in brain image registration. *Neuroimage* 2011;54:2033–2044.
35. Akçakaya M, Weingärtner S, Roujol S, Nezafat R. On the selection of sampling points for myocardial T1 mapping. *Magn Reson Med* 2015;73:1741–1753. doi: 10.1002/mrm.25285.
36. Weingärtner S, Meßner NM, Budjan J, Loßnitzer D, Mattler U, Papavassiliu T, Zöllner FG, Schad LR. Myocardial T1-mapping at 3T using saturation-recovery: reference values, precision and comparison with MOLLI. *J Cardiovasc Magn Reson* 2016;18:126. doi: 10.1186/s12968-016-0302-x.
37. Heidenreich JF, Weng AM, Donhauser J, Greiser A, Chow K, Nordbeck P, Bley TA, Köstler H. T1- and ECV-mapping in clinical routine at 3 T: differences between MOLLI, ShMOLLI and SASHA. *BMC Medical Imaging* 2017 17:1 2019;19:1–9. doi: 10.1186/s12880-019-0362-0.
38. van Heeswijk RB, Feliciano H, Bongard C, Bonanno G, Coppo S, Lauriers N, Locca D, Schwitter J, Stuber M. Free-Breathing 3 T Magnetic Resonance T2-Mapping of the Heart. *JACC Cardiovasc Imaging* 2012;5:1231–1239. doi: 10.1016/j.jcmg.2012.06.010.

39. Yang H-J, Sharif B, Pang J, Kali A, Bi X, Cokic I, Li D, Dharmakumar R. Free-breathing, motion-corrected, highly efficient whole heart T2 mapping at 3T with hybrid radial-cartesian trajectory. *Magn Reson Med* 2016;75:126–136. doi: 10.1002/mrm.25576.

40. Messroghli DR, Moon JC, Ferreira VM, et al. Clinical recommendations for cardiovascular magnetic resonance mapping of T1, T2, T2* and extracellular volume: A consensus statement by the Society for Cardiovascular Magnetic Resonance (SCMR) endorsed by the European Association for Cardiovascular Imaging (EACVI). *J Cardiovasc Magn Reson* 2017;19:75. doi: 10.1186/s12968-017-0389-8.